Phys. Status Solidi B **246**, No. 10, 2216–2231 (2009) / **DOI** 10.1002/pssb.200945169

physica status solidi b
www.pss-b.com
basic solid state physics

Feature Article

Oxide glasses with magnetic nanoparticles: transparent magnets (Faraday rotation and electron magnetic resonance studies)

Irina Edelman[*,1] **and Janis Kliava**[**,2]

[1] L.V. Kirensky Institute of Physics, Siberian Branch of the Russian Academy of Sciences, Akademgorodok 38, 660036 Krasnoyarsk, Russia
[2] Centre de Physique Moléculaire Optique et Hertzienne, Université Bordeaux1–CNRS, UMR 5798, 351 cours de la Libération, 33405 Talence cedex, France

Received 2 April 2009, revised 1 July 2009, accepted 10 July 2009
Published online 20 August 2009

PACS 75.50.Tt, 76.30.Fc, 76.50.+g, 78.20.Ls, 78.67.Bf

[*] Corresponding author: e-mail ise@iph.krasn.ru, Phone: +7 391 2 494 556, Fax: +7 391 2 438 923
[**] e-mail j.kliava@cpmoh.u-bordeaux1.fr

In the first part of this paper we outline the state of the art in the field of magnetic nanoparticles in oxide glasses. We describe the theoretical background of two complementary techniques used for the studies of the state of paramagnetic ions, clusters and magnetic particles in a diamagnetic matrix, *viz.*, magnetooptical Faraday rotation (FR) and electron magnetic resonance (EMR) and we overview previous results obtained with these techniques for several glass systems. In the second part, we highlight the case of potassium-alumina-borate glasses – a glassy system where doping with paramagnetic oxides results in formation of magnetic particles at very low contents of paramagnetic additions: Fe_2O_3 and MnO. In the special case when the ratio of the iron and manganese oxides in the charge is 3/2, magnetic nanoparticles with characteristics close to those of manganese ferrite are formed already at the first stage of the glass preparation. After thermal treatment all glasses show FR and EMR spectra attesting to the presence of superparamagnetic nanoparticles, characterized by relatively broad size and shape distributions. The formation of magnetic nanoparticles confers to these glasses magnetic and magneto-optical properties typical of magnetically ordered substances. At the same time, the glasses remain transparent in a part of the visible and near infrared spectral range and display a high FR value. Such properties make them particularly interesting for use as new media for various magneto-optical devices.

1 Introduction The requirement of modern technology for effective optical device media stimulates investigations of new materials possessing high magneto-optical figure of merit. Glasses containing magnetic particles are promising materials for near infrared spectral range [1, 2]. Owing to its high flexibility, the glass technology is well appropriate for producing nanoparticles with predetermined properties.

To our knowledge, strong interactions between paramagnetic ions in oxide glass matrix were reported for the first time in 1965 (for borate glasses with manganese additions) [3]. Subsequently, a number of authors have focused their attention on the formation of magnetic nanoparticles in glass matrices [4–11], in particular, on peculiar magnetic properties of glasses with nanoparticles, characteristic of magnetically ordered substances and arising from magnetic nanoparticles formed in the course of an additional thermal treatment.

As a rule, in order to obtain magnetic nanoparticles in a glass, a high content of paramagnetic oxide such as Fe_2O_3, MnO or CoO (20–40 mol%) must be introduced into the glass composition. However, some glass systems, partially devitrified by thermal treatment, elude this rule; indeed, nanoparticles of lithium ferrite $LiFe_5O_8$ in lithium

borate glass containing less than 1 mass% Fe_2O_3 [12–16] and nanoparticles of maghemite (γ-Fe_2O_3) in sol–gel silica glass with Fe/Si molar ratio of 2% [16–18] were identified by electron magnetic resonance (EMR). Peculiarities of magnetic susceptibility [19, 20] and Mössbauer spectra [21] of thermally treated potassium-alumina-borate glasses of molar composition $22.5K_2O$–$22.5Al_2O_3$–$55B_2O_3$ containing less than 3.0 mass% of Fe_2O_3 (above 100 mass% of basic glass composition) were related to the formation of ferrite nanoparticles. Later, glasses of this system co-doped with MnO and Fe_2O_3 have been synthesized. After thermal treatment these glasses acquire a non-linear magnetic field dependence of the magnetization with hysteresis and magnetic saturation. At the same time, they retain a high transparency in a part of the visible and near infrared spectral range and demonstrate a high value of the magneto-optical Faraday rotation (FR) [1–2], so that one can refer to them as to 'transparent magnetic glasses'. Such materials are promising media for new magneto-optical data storage devices, optical fibre sensors [22], optical isolators [23, 24], optical voltage sensors [25], *etc*. Meanwhile, the FR values and their spectral characteristics in these glasses largely depend on thermal treatment conditions as well as on absolute and relative concentrations of manganese and iron oxides.

Fabrication of glasses with purposely varied physical properties requires a thorough understanding of mechanisms of the nanoparticle formation at various stages of the glass synthesis and further thermal processing. A number of experimental techniques have been used to study the glasses with nanoparticles, namely, static magnetization and susceptibility measurements, optical and magnetooptical spectroscopy, including FR, Mössbauer spectroscopy, X-ray diffraction, extended X-ray absorption fine structure, transmission electron microscopy, EMR *etc*. In this paper we have deliberately chosen to restrict ourselves to the results obtained by using only two experimental techniques: the FR and the EMR. The reason for this choice, to some extent, is due to our respective personal research interests; meanwhile, it is far from being only subjective. Indeed, the FR and the EMR are expected to yield consistent and complementary data, since they are closely related to each other by the underlying physical phenomenon, *viz*., splitting of electronic energy levels due to breaking the degeneracy in an applied magnetic field. However, this relation is not as intimate as the reader would anticipate from the famous Wikipedia, affirming (in the English, French, Spanish and Italian versions of the appropriate article) that '*The Faraday effect is a result of ferromagnetic resonance*'. In order to dispel this misunderstanding, we remind the reader that, in fact, as schematically illustrated in Fig. 1, the electronic transitions involved in the FR and the EMR are quite different. The former, as a rule, are due to electrical dipole transitions between different orbital states, and they usually occur in the optical wavelength range. On the other hand, the EMR is due to magnetic dipole transitions between different Zeeman sublevels of one and the same orbital state, and it usually occurs in the microwave frequency range.

The FR in glasses doped with transition metal and/or rare-earth oxides includes a positive (diamagnetic) contribution of the glass matrix and a negative (paramagnetic) contribution due to the dopant ions. At low concentrations of the latter the diamagnetic contribution is predominant and the resulting FR has a positive sign. With an increase in the doping level the resulting FR decreases and undergoes a sign change at a certain concentration of the paramagnetic ions. However, such behaviour is observed only for diluted and not for exchange-coupled paramagnetic ions; indeed, clustering and nanoparticle formation cause deviations from this simple picture.

In the vitreous system studied in this work, depending on the composition, thermal treatment and measurement

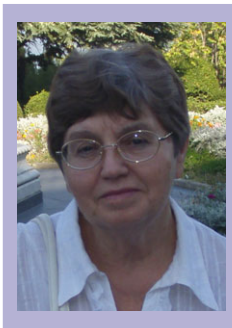

Irina Edelman studied physics and earned her Cand. Sci. degree at the Krasnoyarsk Pedagogical Institute, Russia. Continuing her scientific career at the L.V. Kirensky Institute of Physics of the Siberian Branch of Russian Academy of Sciences, she received her Dr. Sci. degree and successively held staff positions of junior, senior and leading scientist and head of laboratory. Since 2002 she is professor and principal scientist at this Institute. Her research interests include magneto-optical phenomena in 3d and 4f ion compounds, optical and magneto-optical spectroscopy, thin magnetic films and magnetic nanoparticles in non-magnetic matrices. She is constantly surrounded by students and young scientists, and fifteen of them have prepared PhD theses under her supervision.

After graduating from the Moscow University, where he received his Cand. Sci. degree, Janis Kliava worked first as staff researcher and later as professor, head of chair at the University of Latvia, Riga. He received his Dr. Sci. degree from the Institute of Physics of the Latvian Academy of Sciences. In 1993 he accepted the position of professor at the Université Bordeaux-1, France. His scientific activities focus on computer-assisted EMR spectroscopy of diluted ions, clusters and nanoparticles in glasses. He has authored a monograph on 'Electron Paramagnetic Resonance of Disordered Solids' (1984) and, recently, a chapter on 'Electron Magnetic Resonance of Nanoparticles' in the textbook 'Magnetic Nanoparticles' (2009).

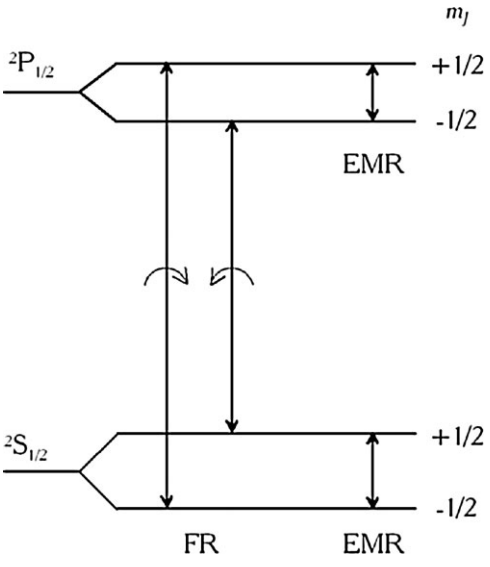

Figure 1 Schematic representation of electronic levels and transitions involved in the FR and the EMR for a hypothetic case of an ion/molecule with the $^2S_{1/2}$ ground state and the $^2P_{1/2}$ excited state.

temperature, both the electron paramagnetic resonance (EPR) of isolated ions and the superparamagnetic resonance (SPR) of magnetically ordered nanoparticles can be observed. The generic term of EMR encompasses both of these resonances.

The EMR spectra in such glasses not subjected to an additional heat treatment usually exhibit well-separated features: the 'low-field' ones, most often arising at the effective g-values $g_{\text{eff}} = 4.3$, 6.0 and 9.7 and the 'high-field' ones at $g_{\text{eff}} \approx 2.0$ [26–32]. The low-field features are due to the EPR of diluted ions in heavily distorted surroundings and they provide detailed information on the closest environment of these ions. On the other hand, the resonances in the vicinity of $g_{\text{eff}} \approx 2.0$ can arise both from isolated ions in less distorted environment and from clusters or nanoparticles [26, 32]. Note that in some earlier EMR studies of crystallization of glasses the latter distinction had not been recognized, and the disappearance of the low-field features accompanied by a narrowing of the $g_{\text{eff}} \approx 2.0$ one had been ascribed solely to the removal of random distortions in the environment of the paramagnetic ions, while possible clustering and nanoparticle formation were ignored, *e.g.*, see Ref. [33]. In fact, distinguishing between these two possibilities requires thorough variable-temperature studies, as carried out in the present work.

2 Bibliographical synopsis

2.1 Magnetic nanoparticles in glasses The first report on strong interactions between paramagnetic synopsis ions in oxide glass matrix (borate glasses with Mn additions) refers to 1965 [3]. Since then many authors have shown their interest in the formation of magnetic particles in the glasses [4–9, 34–37]. Thus, antiferromagnetic ordering was observed in phosphate glasses activated with Cr, V or Mn [37], Fe [4, 35] and in glasses based on P_2O_5 and containing high concentrations (up to 40 mass%) of Mn, Fe, Ni, Co, and Cu [38, 39]. However, in most of these studies the nanoparticle formation was considered only hypothetically, as one of possible reasons of peculiar characteristics of the glasses. Probably, for the first time magnetic nanoparticles in the glasses were reliably identified in the Li_2O–Na_2O_3–Fe_2O_3–B_2O_3 system containing from 15 to 49 mass% Fe_2O_3, by using a combination of experimental techniques: magnetic susceptibility, Mössbauer spectroscopy, X-ray diffraction, EMR and ultrasound velocity [38]. As the iron concentration increased, the magnetic characteristics of the glasses transformed from paramagnetic to superparamagnetic ones. At Fe_2O_3 contents about 30 mass% a hyperfine structure appeared in the Mössbauer spectra, attesting to the presence of crystalline oxides γ-Fe_2O_3, α-Fe_2O_3 and Fe_3O_4. The α-Fe_2O_3 phase was also identified in the X-ray diffraction pattern.

The phase separation was clearly observed in BaO–B_2O_3–Fe_2O_3 glasses subjected to thermal treatment at 590 °C [40]. The magnetization curves at different temperatures (77–293 K) were shown to coincide when plotted versus magnetic field over temperature, as expected for an assembly of superparamagnetic particles with blocking temperature below 77 K. The particle radii were estimated as 1–3 nm. A longer thermal treatment time resulted in an increase of the particle magnetic moments and a decrease of their numbers. The temperature dependence in the 15–300 K range of the magnetic susceptibility of alumina-silicate glasses with high concentrations of Co or Mn could be well described assuming the existence of antiferromagnetically ordered single domains of *ca.* 100 nm in size [5]. It should be noted that manganese-containing glasses are of interest from the viewpoint of their electric properties. In this relation, much attention was paid to the glass synthesis and to manganese valence and coordination states. De Bufala [41] concluded that manganese was incorporated in glasses as Mn^{2+} or Mn^{4+} ions. The magnetic properties of $0.05Li_2O$–$0.15MnO$–$0.15Fe_2O_3$–$0.65SiO_2$ and $0.37Na_2O$–$0.26Fe_2O_3$–$0.37SiO_2$ glasses were explained by formation of antiferromagnetic particles [34]. Cobalt ferrite particle formation was studied by a combination of experimental techniques in CaO–B_2O_3–Fe_2O_3–CoO glasses for the anneal temperatures between 400 and 900 °C [5]. The particles had linear dimensions between 26 and 210 nm and specific saturation magnetizations between 74 and 88 Am^2/kg, and their magnetization was characterized by hysteresis loops.

Nanosized magnetite Fe_3O_4 crystallites were prepared by thermal treatment of a rapidly quenched silicate glass melt of composition $27.4CaO$–$42.8SiO_2$–$6.1B_2O_3$–$23.7Fe_2O_3$ (in mol%) [7]. Small-angle neutron scattering experiments of samples annealed at different heat treatment conditions were performed in order to determine the evolution and nature of a nonmagnetic surface shell of the nanocrystals enriched with structurally distorted Fe_2O_3 and growing at the

expense of the magnetite core by oxidizing the surface of the nanocrystals.

In thermally treated metastable oxide glass ribbons prepared by rapid quenching of Fe_2O_3–BaO–B_2O_3–Sb_2O_3 melt between rotating copper rollers, nanocrystals of lithium ferrite $LiFe_5O_8$ were detected by X-ray diffraction, scanning electron microscopy and magnetization measurements [10]. An increase of average nanocrystal size from 3.5 to 50 nm was observed with increasing the anneal temperature from 440 to 770 °C.

Rapid quenching technique was also used to prepare glasses of nominal compositions $Sr_{0.6}La_{0.4}Fe_{11}6Co_{0.4}O_{19} + 12SrB_2O_4$, $SrFe_{12}O_{19} + nNa_2Sr_2B_4O_9$ ($n = 4$, 6, 8, 10) and $SrFe_{12}O_{19} + 6Na_2Sr_3B_4O_{10}$ from oxide melts [42, 43]. After a thermal treatment at temperatures from 550 to 900 °C glass-ceramics were formed containing fine lanthanum and cobalt-doped strontium hexaferrite $SrFe_{12}O_{19}$ particles. The coercivity of the glass-ceramic samples increased up to 486 kA/m with increasing the treatment temperature. The specific saturation magnetization of samples increased up to 25 Am^2/kg as the heat treatment temperature was increased to 750 °C, and slightly decreased at higher temperatures. Dissolving the nonmagnetic matrix of the glass-ceramic prepared at 900 °C, a submicron powder of composition $Sr_{0.88}La_{0.12}Fe_{10.74}Co_{0.47}O_y$ was obtained, as determined by X-ray microanalysis.

Formation of barium hexaferrite $BaFe_{12}O_{19}$ nanoparticles was observed in B_2O_3–BaO–Fe_2O_3 [44] and 35% BaO–35%Fe_2O_3–20%B_2O_3–10% SiO_2 (mol%) [45] glasses prepared by cooling the melts between steel rollers. Considerable attention was paid to the effect of ZrO_2 or SiO_2 admixtures on crystallization, microstructure and magnetic properties of BaO–Fe_2O_3–B2O_3–SiO_2 glass ceramics [46]. A one-stage heat treatment of the glass ribbons resulted in a non-uniform particle distribution, while a two-stage treatment at 526 and 721 °C generally led to a more uniform distribution of platelet particles. Pressed powders showed the finest and the broadest size distribution of acicular and platelet particles. All samples showed nearly identical values of saturation magnetization of 25–27 emu/g while the coercivity varied between 2800 and 3800 Oe. An addition of ZrO_2 apparently resulted in a quite distinct glass-in-glass phase separation in as-prepared samples, significantly affecting the nucleation process.

Glasses of $x$$Fe_2O_3$–(80.0−$x$)$Bi_2O_3$–20.0$B_2O_3$ ($18.2 \leq x \leq 40.0$) and 32Fe_2O_3–48Bi_2O_3–20B_2O_3 compositions were prepared from reagent grade Fe_2O_3, Bi_2O_3, and B_2O_3 powders by using a conventional melt-quenching method [47, 48]. The glasses manifested intriguing magnetic behaviour explicable in terms of coexistence of a spin glass phase and magnetic clusters. The $x = 18.2$ glass showed a spin glass transition at 3.5 K, while the contribution of magnetic clusters to the magnetic properties became more significant at increased x. For the glass with $x = 32.0$ two different magnetic transitions were observed, as demonstrated by temperature and frequency dependences of the magnetic susceptibility. The studies of magnetic ageing and memory effects showed that the magnetic clusters were frozen and formed a super spin glass-like state with strong intercluster interactions at low temperatures. The transmission electron microscopy showed that the structure of these clusters was rather amorphous than crystalline. From the observation of exchange bias effects it was concluded that the interplay between the clusters and the spin glass phase brought about an exchange anisotropy field after cooling in the presence of magnetic field.

The above synopsis covers the field of glasses synthesized with conventional rapid quenching technology and does not include non-crystalline materials prepared using other techniques, *e.g.*, sol–gel silica glasses.

2.2 Magneto-optical Faraday effect The angle of rotation α of the plane of polarization of light in a material is given by the well-known equation

$$\alpha = VlB, \tag{1}$$

where l is the length of the light path in the matter, B is the magnetic field applied along the light beam and V is the Verdet constant. In the general case this constant includes three contributions [49, 50]:

$$V = -\frac{4\left(n^2+2\right)^2}{9nc} N\omega^2 \left[g\left(\omega, \omega_{mn}\right) a + f\left(\omega, \omega_{mn}\right) \times \left(b + \frac{c}{kT}\right)\right], \tag{2}$$

where n is the average refractive index, c the speed of light, N the number of optically active centres, ω_{mn} the angular frequency of transition between n and m states, g and f lineshapes, k the Boltzmann constant and T is the temperature. In Eq. (2) the temperature-independent 'diamagnetic' term in a arises from the Zeeman splitting of electronic levels in an external magnetic field; the 'paramagnetic' term in c is due to the difference of populations of the ground state magnetic sublevels and the term in b is due to the perturbation of the wave functions of the m and n states in the magnetic field through an admixture of wave functions of closely lying levels.

In the case of paramagnetic and, *a fortiori*, ferromagnetic or ferrimagnetic substances, the term in c gives the predominant contribution to V, and it can be rewritten as

$$V_{\text{para}} \approx 2\pi \frac{e^2}{m} \Delta N_{nm} \frac{E_{nm}^2 - E^2}{\left(E_{nm}^2 - E^2\right)^2 + E^2\gamma^2}, \tag{3}$$

where e and m are the electron charge and mass, respectively, ΔN_{nm} the difference between number of atoms in n and m levels, $E_{nm} = \hbar\omega_{nm}$ the energy difference between the n and m states and γ is the linewidth.

Numerous electron transitions can contribute to the FR. First of all, these are allowed electric dipole transitions,

typically occurring in the visible or ultraviolet spectral range. Namely, these transitions provide a high FR value in the visible range for compounds of several 4*f* ions, *e.g.*, Tb^{3+}, Dy^{3+} and Eu^{2+}, justifying the great attention paid to the FR of glasses containing such ions [51–55]. On the other hand, glasses with 3*d* ions even at low doping levels (a few mol%) often show an intense absorption in the visible range, making it difficult to study the FR in these glasses. However, we can mention here an interesting example of phosphate glasses xFeO–(100−x)P_2O_5 with $x = 50.0$, 54.0 and 57.1 mol% [56]. These glasses exhibited fairly high transmittance in the visible range and large FR at the wavelength of *ca.* 400 nm. The ^{57}Fe Mössbauer spectra confirmed that almost all iron ions in these glasses were present as Fe^{2+}, and an intense optical absorption in the ultraviolet and infrared wavelength ranges was ascribed, respectively, to a charge transfer transition from O^{2-} to Fe^{2+} and to a *d*–*d* transition. The analysis of the FR wavelength dependence using the Van Vleck-Hebb theory [57] had revealed that the charge transfer transition contributed more significantly to the FR owing to the large effective transition probability, comparable to those reported for glasses containing 4*f* rare-earth ions. The magneto-optical figure of merit showed a maximum of about 13° at *ca.* 380 nm.

The intra-configuration transitions (*f*–*f* for the rare-earth ions and *d*–*d* for the 3*d* ions), parity-forbidden and often spin-forbidden, as a rule, only slightly perturb the smooth curve of Eq. (3) in the vicinity of the transition energy. However, in compounds with magnetic order the intensity of the *d*–*d* transitions can be greatly enhanced by the interaction between the magnetic and electronic subsystems. In particular, magnetic nanoparticles dispersed in the glass matrix are expected to provide significant FR values in spectral regions corresponding to one or another electron transition. For the Fe_3O_4 nanoparticles, the maximum of FR should occur at *ca.* 750 nm, this wavelength corresponding to the spin-allowed $^5T_2$–^5E transition in Fe^{2+} ions of $3d^6$ configuration, as have been observed for Fe_3O_4 thin films [58]. In the case of $3d^5$ Mn^{2+} and Fe^{3+} ions, one can expect to observe contributions to the FR in the 600–1500 nm range from electronic transitions $^6A_1$–$^4T_1$, $^6A_1$–$^4T_2$, $^6A_1$–$^4A_1$, ^4E in tetrahedral coordination and $^6A_{1g}$–$^4T_{1g}$, $^6A_{1g}$–$^4T_{2g}$, $^6A_{1g}$–$^4A_{1g}$, ^4E_g in octahedral coordination, as, indeed, has been the case for manganese ferrite thin films [58–60].

2.3 Electron magnetic resonance The free energy of a single-domain particle of ellipsoidal form with a magnetic moment μ to first order in the magnetic symmetry can be expressed as, *cf.*, *e.g.*, [61]:

$$E = -\mu \cdot B + K_1 V \Phi_V + K_S S \Phi_S + \frac{1}{2}\frac{\mu_0}{V}\boldsymbol{\mu} \cdot \boldsymbol{N} \cdot \boldsymbol{\mu}. \quad (4)$$

Here the first term is the Zeeman energy, the second term is the first-order magnetocrystalline anisotropy energy proportional to the particle volume V and to the corresponding constant K_1, the third term describes the contribution of the particle surface proportional to its area S and to the surface anisotropy constant K_S and the fourth term is the magnetostatic energy with $\boldsymbol{N}$ the demagnetizing tensor. The latter three terms depend on the orientation of $\boldsymbol{\mu}$ with respect to the magnetic symmetry axes, described by the directional cosines l_x, l_y, l_z or by the polar and azimuthal angles α and β of $\boldsymbol{\mu}$. The function Φ_V depends on the magnetic symmetry; namely, in cubic symmetry

$$\Phi_V\left(l_x, l_y, l_z\right) = l_x^2 l_y^2 + l_x^2 l_z^2 + l_y^2 l_z^2, \quad (5)$$

and in axial symmetry

$$\Phi_V\left(l_x, l_y, l_z\right) = 1 - l_z^2. \quad (6)$$

The surface anisotropy is also supposed to be of axial symmetry, *e.g.*, see Refs. [62, 63].

The equilibrium orientation of $\boldsymbol{\mu}$ minimizes the value of E, and for small departures from equilibrium the resonance magnetic field can be calculated from the following equation [64]:

$$B_0^2 = \frac{1}{\mu^2}\left(E_{\alpha\alpha}E_{\beta\beta} - E_{\alpha\beta}^2\right), \quad (7)$$

where $B_0 = -\omega/\gamma$, ω is the angular frequency of the microwave radiation, $\gamma<0$ is the gyromagnetic ratio and $E_{\alpha\alpha}$, $E_{\beta\beta}$ and $E_{\alpha\beta}$ are shortcuts for

$$E_{\alpha\alpha} = \left(\frac{\partial^2 E}{\partial\alpha^2}\right)_0; \quad E_{\beta\beta} = \left(\frac{1}{\sin^2\alpha}\frac{\partial^2 E}{\partial\beta^2} + \mathrm{ctg}\alpha\frac{\partial E}{\partial\alpha}\right)_0;$$
$$E_{\alpha\beta} = \left(\frac{1}{\sin\alpha}\frac{\partial^2 E}{\partial\beta\partial\alpha} - \frac{\mathrm{ctg}\alpha}{\sin\alpha}\frac{\partial E}{\partial\beta}\right)_0. \quad (8)$$

The subscript 0 indicates that the corresponding derivatives and trigonometric functions are calculated at equilibrium.

The 'classical' description outlined above has been reformulated by Noginova et al. in terms of the quantum mechanics, considering the magnetic nanoparticle as a single giant spin [65]. In this approach the EMR spectrum is calculated as the sum of contributions from the transitions between different spin levels. However, in the present state of the art this model seems to be in disagreement with a number of important EMR in typical nanoparticle systems. For instance, it is expected to yield the Curie-type $1/T$ dependence of the total EMR intensity, in contradiction with the experimentally observed tendency; *vide infra*. Besides, it does not account for the characteristic asymmetry of low-temperature EMR spectra. The framework of the present paper does not allow a detailed analysis of the Noginova's et al. model, so, it will be published elsewhere.

In the case of nanosized particles, the magnetic anisotropy energy becomes comparable to/smaller than kT. At elevated temperatures, thermal fluctuations of the magnetic moments severely reduce both the angular anisotropy of resonance magnetic fields and the intrinsic

linewidths. As a result, in macroscopically isotropic nanoparticle systems the EMR spectra exhibit spectacular temperature-dependent narrowing, which is the more pronounced the smaller is the particle size. In order to differentiate the particular type of nanoparticle magnetic resonance, on the one hand, from the EPR of diluted ions and, on the other hand, from the ferromagnetic or antiferromagnetic resonance in bulk magnetic materials, we refer to it as the SPR. The latter term, apparently, has been first used by Sharma and Waldner to describe peculiarities of the EMR spectra of Fe_3O_4 nanoparticles in ferrofluids [66], namely, emergence of the characteristic 'two-line pattern', *viz,* a superposition of a broad and a narrow line, both centred at $g_{\text{eff}} \approx 2$.

A simple 'intuitive' way to account for this particle volume-dependent narrowing of the SPR spectra, suggested by de Biasi and Devezas [67], consists in 'renormalizing' the magnetic parameters by averaging over the motion caused by thermal fluctuations of the magnetic moments. This averaging is expressed by means of the Langevin function family, as follows:

$$\langle M \rangle = M \langle \cos\alpha \rangle = M \langle P_1(\cos\alpha) \rangle = M \mathfrak{L}_1(x) = M \left(\coth x - \frac{1}{x} \right), \tag{9}$$

and

$$\langle K_1 \rangle = K_1 \langle P_n(\cos\alpha) \rangle = K_1 \mathfrak{L}_n(x), \tag{10}$$

where $P_n(\cos\alpha)$ are the n-th order Legendre polynomials and the angular brackets denote averaged quantities, $x = \mu B/kT$ and $\mathfrak{L}_1(x)$ is the 'usual' Langevin function. In the case of axial, $n = 2$ and cubic, $n = 4$ magnetic symmetry one gets, respectively

$$\langle P_2(\cos\alpha) \rangle = \mathfrak{L}_2(x) = 1 - \frac{3}{x}\mathfrak{L}_1(x), \tag{11}$$

and

$$\langle P_4(\cos\alpha) \rangle = \mathfrak{L}_4(x) = 1 - \frac{10}{x}\mathfrak{L}_1(x) + \frac{35}{x^2}\mathfrak{L}_2(x). \tag{12}$$

The Biasi and Devezas approach, in fact, is a particular case of a more general model developed by Raikher and Stepanov [68, 69] and based on the theory of thermal fluctuations in magnetic particles by Brown [70].

The emergence of exchange-coupled clusters has been inferred from combined EMR, Mössbauer effect and optical absorption studies of $40Na_2O$–$60SiO_2$ silicate glasses and $20K_2O$–$40ZnO$–$40P_2O_5$ phosphate glasses containing up to 5.0 mol% of Fe_2O_3 [26] and from EMR and magnetic susceptibility studies of xFe_2O_3–$(1-x)(BaO$–$4B_2O_3)$, $0 < x < 0.1$, borate glasses [27]. However, no thermal treatment was performed and no temperature dependences of the EMR spectra were reported for these systems.

Berger et al. [12–14] carried out a series of studies of borate glass of the molar composition $0.63B_2O_3$–$0.37Li_2O$ containing very low amount of Fe_2O_3, 0.75×10^{-3} mol%. The glasses were treated by repeated stages for 1/2 h at increasing anneal temperatures T_a starting at the glass transition temperature $T_g = 708$ K. The as-prepared glass exhibited an asymmetric EPR feature at $g_{\text{eff}} \approx 4.3$ accompanied by a plateau extending towards low magnetic fields with a shoulder at $g_{\text{eff}} \approx 9.7$, characteristic of isolated Fe^{3+} ions. As T_a increased, this spectrum gradually decreased in intensity and finally disappeared. Simultaneously, a new resonance emerged at $g_{\text{eff}} \approx 2.0$, appearing as a narrow line superposed with a broader one (the 'two-line pattern'). The narrow component predominated at lower T_a and it was progressively replaced by the broader one at higher T_a. Such behaviour is indicative of the devitrification process, as confirmed by X-ray diffraction results. In the spectra recorded at higher temperatures from 300 to 723 K, a spectacular dynamical narrowing of the spectra, a hallmark of the SPR, was observed [14].

Numerical integration of the experimental EMR spectra showed that in the course of the heat treatment the resonance intensity increased at least by two orders of magnitude, indicating the *change of the nature of the resonance* – from the EPR of isolated ions to the SPR of iron-containing magnetic nanoparticles.

Because of the very low iron content, no iron-containing phases could be observed by X-ray diffraction, but nanoparticles arising in annealed borate glasses with higher iron oxide contents were identified by X-ray diffraction as lithium ferrite $LiFe_5O_8$ [71]. Kliava and Berger carried out computer simulations of the nanoparticle SPR spectra in the borate glass with the magnetic parameters of lithium ferrite using the approach based on the joint distribution density $P\left(d, n_{\parallel}\right)$ of the particle diameters and demagnetizing factors [16–18, 29] (where, for a spheroidal particle, the latter are defined as follows: $N_{\parallel} = \frac{1}{3} + n_{\parallel}$ and $N_{\perp} = \frac{1}{3} - \frac{1}{2}n_{\parallel}$). They concluded that with the increase of the anneal temperature, the most probable diameter d_0 of the magnetic nanoparticles increased while the standard deviation σ_d decreased, so that the assembly of nanoparticles became more ordered. The absolute values of mean demagnetizing factors, n_0, remained small in comparison with the corresponding distribution widths σ_{n_z} indicating random distortions of the nanoparticle shapes from that of a sphere with no marked preference for any average distortion.

In spite of the very specific shape of the joint distribution density $P\left(d, n_{\parallel}\right)$, the marginal distribution density of nanoparticle diameters $P_m(d)$ was shown to be *unimodal*. It might seem surprising that such distribution could well reproduce the 'two-line pattern' in the SPR spectrum. In fact, one deals here with a specific example of a very general characteristic of magnetic resonance spectra of disordered systems: singularities (sharp features) appear in such spectra if the resonance magnetic field is stationary with respect to the distributed magnetic parameters [72]. This situation is similar to that of the EPR spectra of diluted Fe^{3+} or Gd^{3+}

Table 1 MnO concentrations in samples containing 1.5 mass% of Fe_2O_3 in the batch.

sample number	MnO, mass%
1	0
2	0.2
3	0.4
4	0.9

ions in oxide glasses, *viz*. a unimodal distribution of the fine structure parameters, brought about by disorder inherent in the vitreous state, gives rise to several well-defined resonance lines. In the present case, such singularity is typified by the sharp $g_{\text{eff}} \approx 2.0$ feature, arising from smaller magnetic nanoparticles for which the anisotropy and demagnetizing magnetic fields are almost entirely averaged by thermal fluctuations of their magnetic moments.

3 Transparent magnetic glasses

3.1 Experimental details KNO_3, Al_2O_3 and H_3BO_3 in proper concentrations were used as initial materials to fabricate glasses with the basic composition $22.5K_2O$–$22.5Al_2O_3$–$55B_2O_3$ according to the technique described in Ref. [1].

Two series of samples have been prepared:

(i) Before synthesis, 1.5 mass% of Fe_2O_3 and various concentrations of MnO over 100 mass% of the basic composition, see Table 1, were added to the charge. The mixtures were melted at 1100 °C in oxidizing conditions, poured onto steel sheets, cooled naturally in air to 380 °C and maintained at this temperature for several hours. Additional thermal treatment was carried out at 560 °C during 2 h.

(ii) Fe_2O_3 and MnO in respective concentrations 3.0 mass% and 2.0 (sample 5) or 2.5 (samples 6 and 7) mass% were added to the charge. The preparation details were the same as for the series (i), save that sample 6 was melted at 1000 °C. Samples 5–7 were subjected to three kinds of additional thermal treatment, *viz*., at 560 °C, at 600 °C (both during 2 h) and at two steps: first at 560 and next at 600 °C, during 2 h at each temperature. The MnO concentrations as well as the synthesis and additional thermal treatment temperatures for different samples are shown in Table 2.

The FR measurements were made with optically smoothed samples (1.0 ± 0.05) mm thick. For the EMR measurements rectangular samples with dimensions $2 \times 3 \times 4$ mm^3 were used.

The EMR spectra were recorded in the temperature range from 4.2 to 300 K in the X band (9.46 GHz) with a Bruker EMX spectrometer equipped with an ER4112HV variable temperature unit.

3.2 Faraday rotation

3.2.1 As-prepared samples Curve 1 in Fig. 2 (both left and right) has been measured with a glass containing no paramagnetic additions. This curve is well described by the diamagnetic term in Eq. (2), and the corresponding positive contribution to the Verdet constant is denoted by V_{dia}. Curves 2 and 3 in Fig. 2 left show, respectively, the spectral dependences of the Verdet constant and of the paramagnetic contribution $V_{\text{para}} = V - V_{\text{dia}}$ for as-prepared samples 1–4 containing 1.5 mass% Fe_2O_3. (The results for samples 1–4 are practically undistinguishable.) All these samples also have positive Verdet constants, and the fact that their V values are less than V_{dia} is due to the negative sign of V_{para}.

For isolated (non-interacting) ions V_{para} is expected to increase in proportion to their concentration. The obvious non-observance of this rule shows that in the present case these ions are not isolated but coupled, presumably by indirect antiferromagnetic exchange through oxygen ions. Such ions do not contribute to the FR in the applied magnetic field range. A similar situation occurs for samples 6 and 7; the V_{para} values for these samples coincide with each other (curve 2 in Fig. 2 right) and are close to V_{para} for sample 3 (curve 3 in Fig. 2 left) in spite of significantly higher concentrations of paramagnetic additions in the former samples in comparison with sample 3.

The FR spectrum of sample 5, see curve 3 in Fig. 2 right, is fundamentally different from those of all other samples. The total FR (*i.e*., that of the glass matrix plus that of the

Table 2 MnO concentrations in samples containing 3.0 mass% of Fe_2O_3, synthesis (T_s) and thermal treatment (T_t) temperatures, FR value α (for $\lambda = 800$ nm and magnetic field 0.2 T), relative remnant FR α_0/α, and coercive field B_c.

sample	MnO, mass%	T_s, °C	T_t, °C	FR, deg cm^{-1}	α_0/α	B_c, T
5	2.0	1100	560	20.7	0.37	0.009
			600	2.9	0.02	0.007
			560 + 600	23.9	0.39	0.011
6	2.5	1000	560	13.7	0.32	0.012
			600	10.7	0.20	0.010
			560 + 600	12.3	0.31	0.010
7	2.5	1100	560	9.2	0.25	0.009
			600	10.7	0.30	0.011
			560 + 600	16.3	0.39	0.010

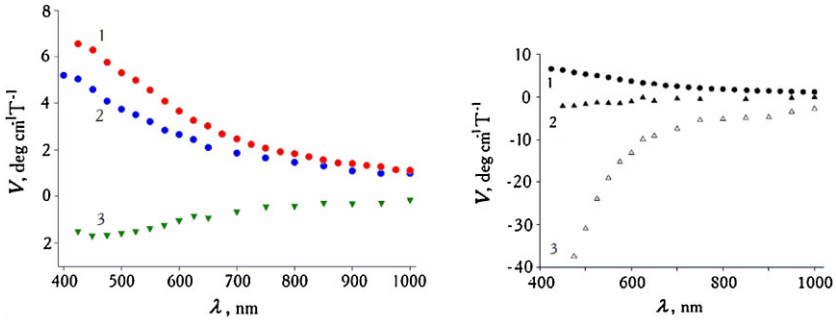

Figure 2 (online colour at: www.pss-b.com) Spectral dependences of the Verdet constant in as-prepared glasses. Left: (1) basic glass without paramagnetic additions, (2) sample 3 and (3) the paramagnetic contribution (V_{para}) in sample 3. Right: (1) same as (1) on the left, (2) and (3) the paramagnetic contributions (V_{para}) in samples 6 and 5, respectively.

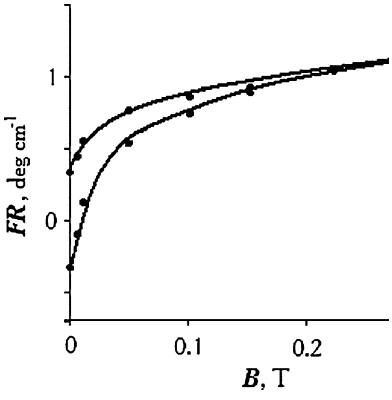

Figure 3 Magnetic field dependence of the FR in as-prepared sample 5 at room temperature and 800 nm wavelength.

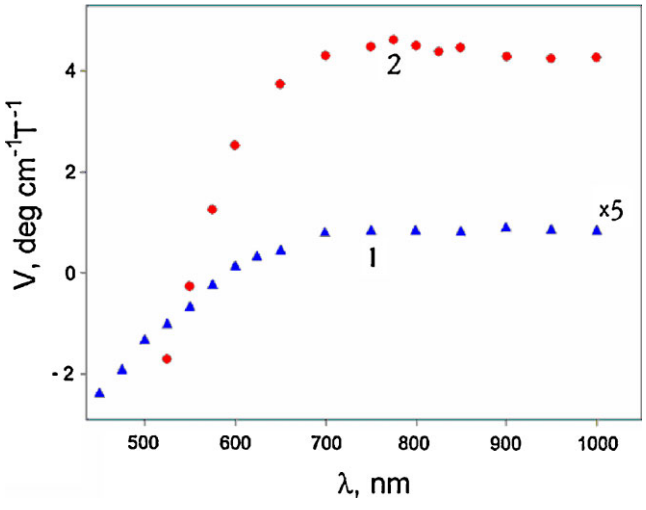

Figure 4 (online colour at: www.pss-b.com) Spectral dependences of the Verdet constant in thermally treated samples. The curves (1) and (2) refer, respectively, to samples 1 and 3 subjected to the thermal treatment at 560 °C during 2 h.

paramagnetic additions) in this sample is negative and its absolute values in the shorter wavelength range are about an order of magnitude larger than in samples 6 and 7, while the total amount of paramagnetic oxides in sample 5 is even less than in the latter ones. Strictly speaking, in this case the contributions to the FR values of manganese and iron additions can no more be referred to as paramagnetic. The shape of the FR spectral dependence in this sample is similar to that of ferrimagnetic materials containing Fe^{3+} and/or Mn^{2+} ions, such as $FeBO_3$ [59], γ-Fe_2O_3 and $MnFe_2O_4$ [60]. The strong FR increase in sample 5 infers an inhomogeneous distribution of Fe and Mn ions in the glass matrix with formation of magnetically ordered (ferro- or ferrimagnetic) particles. This inference is further confirmed by the non-linear magnetic field dependence of the FR for this sample, with hysteresis, see Fig. 3. For samples 6 and 7 the FR value is a linear function of the magnetic field up to 0.5 T, similar to samples 1–4. These results suggest the formation of magnetic particles in sample 5 but yield no unambiguous data on the magnetic state of paramagnetic additions in other samples.

3.2.2 Thermally treated samples Thermal treatment results in substantial changes in the FR: for all samples it becomes negative in the short wavelength range and dramatically increases in absolute value. Therefore, the contribution of the diamagnetic glass matrix to the FR can be neglected in this case. For samples 1–4 the sign of the FR changes in the spectral range of 550–850 nm. For samples 1 and 3 this change occurs at about 550 nm, see Fig. 4. Particularly high FR values are observed for sample 3 in the long wavelength range 600–1000 nm.

For samples 5–7 thermal treatment results in an increase of the optical absorption in the short wavelength part of the spectrum, therefore, the FR has been measured beginning from *ca.* 600 nm. In the whole wavelength range the FR is negative; its absolute values are significantly larger than in samples 1–4 and sharply decrease with the increase in wavelength, see Fig. 5. The FR spectra for samples 5–7 coincide in shape with each other for all treatment regimes. Meanwhile, the modification of the FR values under thermal treatment depends on the Fe and Mn concentration, the glass synthesis temperature and treatment regime.

As far as the FR spectral dependences are similar for samples 5–7 at all thermal treatment regimes used, we can compare the FR values in different samples at one and the same wavelength. Table 2 shows the corresponding FR values at $\lambda = 800$ nm. One can see that in sample 6 a drastic FR change comparing to as-prepared sample occurs already under the treatment at 560 °C, while the treatment at 600 °C

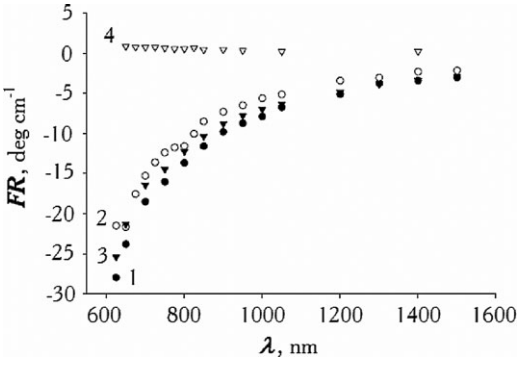

Figure 5 Spectral dependences of the FR in the magnetic field $B = 0.2$ T for as-prepared and thermally treated sample 6. The curve numbers correspond to the treatment at the following temperatures: (1) 560, (2) 600, (3) 560 + 600 °C and (4) as-prepared sample.

and the two-step treatment result in somewhat less change. In sample 7 the treatment at 600 °C produces a little more change in the FR in comparison with that at 560 °C. The increase in the absolute FR value is particularly pronounced for the two-step treatment. The most interesting behaviour is observed in sample 5: the treatment at 560 °C leads to a spectacular FR change which is only slightly enhanced after an additional treatment at 600 °C in the two-step process. In contrast, after the treatment directly at 600 °C the FR value remains close to that of as-prepared sample.

The FR dependences on the external magnetic field for all thermally treated samples are similar, showing a sharp increase at relatively low fields and a slow increase at higher fields. Besides, a magnetic hysteresis is observed, and the characteristics of the hysteresis loop, in particular, the relative remnant FR value α_0/α (where α_0 is the FR in zero magnetic field) and, to a lesser extent, the coercive field B_c correlate with the high-field FR value (Table 2).

The FR values and their spectral and magnetic field dependences in thermally treated samples are characteristic of ferromagnetic or ferrimagnetic substances possessing macroscopic magnetic moments. Meanwhile, because of low contents of the paramagnetic additions in the glasses, magnetic order cannot exist in the whole sample volume. The lack of proportionality between the FR values and the concentration of paramagnetic additions in as-prepared samples suggests that magnetic clusters and even nanoparticles are formed already in as-prepared glasses (in particular, in sample 5). Under thermal treatment these fine particles can act as germs for the formation of larger magnetically ordered particles.

The particle characteristics such as sizes, shapes and structure are extremely sensitive to the thermal treatment regime, to relative and absolute concentrations of paramagnetic additions and, to a lesser degree, to the synthesis conditions. An interesting finding is that for the ratio of iron and manganese oxide concentrations close to 3/2 (sample 5) the nanoparticles already arise during the glass synthesis. Under additional thermal treatment at 560 °C the existing particles gradually increase in size and new particles are formed. As a result, the FR reaches very high values, see Table 2. A subsequent treatment at 600 °C brings about the formation of smaller particles (see Fig. 8 in Ref. [2]) leading to a further FR increase. In samples directly treated at 600 °C the particle growth is impeded and the FR value remains almost the same as in as-prepared sample. For a different Fe and Mn oxide ratio (samples 6 and 7) the particle sizes apparently increase under all three treatment regimes; meanwhile the maximal FR value is only about a half of that in sample 5.

This difference in behaviour between sample 5 on the one hand and samples 6 and 7 on the other hand indicates the essential role played by Mn in oxidizing-reducing conditions during the glass synthesis and hence in the nanoparticle formation process. Indeed, several authors have noted a significant influence of Mn oxide additions on the structure and properties of glasses. For instance, MnO additions enhance crystallization of sodium silicate glasses [73]. The influence of the Mn content on the character of bonds has been demonstrated for $MnO–P_2O_5–TeO_2$ [74, 75] and alkali fluoroborate glasses [76]. However, it should be mentioned that the mechanisms of this influence are different for different glass systems and compositions. A detailed study of particle formation mechanisms in manganese-containing oxide glasses is in progress.

In the glasses studied here, the nature of paramagnetic additions – Fe and Mn –suggests as the most likely candidates for the structure of the magnetically ordered phase, iron oxides such as hematite α-Fe_2O_3, maghemite γ-Fe_2O_3, magnetite Fe_3O_4 or manganese ferrite $Mn_xFe_{3-x}O_4$. The FR spectra for these substances, with the exception of Fe_3O_4, are very similar, see, for instance the data for thin films of γ-Fe_2O_3 and $Mn_xFe_{3-x}O_4$ for different x values [60]. Meanwhile, in contrast to our results for samples 1–4, in the FR spectra of γ-Fe_2O_3 and $Mn_xFe_{3-x}O_4$ a deep minimum is observed near 500 nm, followed by a monotonous decrease in the absolute value in the range down to 2500 nm [60], and the FR values remain negative in the whole spectral range studied. On the other hand, in the FR spectrum of Fe_3O_4 two peaks are observed at *ca*. 480 (negative) and 730 nm (positive) [58]. The latter spectrum is very similar to those of thermally treated sample 3, *cf*. Fig. 4. It can be concluded that in this case the crystal structure of the nanoparticles formed in the glass is closely related to that of magnetite. For other samples in the 1–4 series the FR values in the red part of the spectrum significantly decrease in comparison with that of sample 3 while in the blue part of the spectrum the FR values remain roughly equal for all samples. These results suggest that different types of particles are formed in different samples, *viz*., Fe_3O_4 and γ-Fe_2O_3 or $Mn_xFe_{3-x}O_4$ in samples 1–4 and $Mn_xFe_{3-x}O_4$ in samples 5–7.

We can compare the FR values obtained for the potassium-alumina-borate glasses with the only available data for more-or-less similar materials. Bentivegna et al. [24] reported optical and magneto-optical characteristics of γ-Fe_2O_3 nanoparticles frozen in silica glass matrices. This system was shown to exhibit in the 1.5–2.6 eV (830–500 nm)

spectral range the FR of the same order of magnitude as $Y_3Fe_5O_{12}$, a compound widely used for magneto-optical applications. Bentivegna et al. considered this material to be very useful for applications such as optical rotators, isolators and modulators, based on magneto-optical principles. The glasses studied in the present work are not very transparent in this spectral range; on the other hand, they demonstrate promising optical and magneto-optical properties in the range of 800–1550 nm, also important for practical applications. In particular, the FR of sample 5 at 800 nm is about an order of magnitude larger than that shown in Fig. 3 of Ref. [24]. Another interesting property of these glasses is a relatively large remnant FR, see Table 2.

3.3 Electron magnetic resonance

3.3.1 As-prepared samples The EMR spectra of as-prepared samples, *e.g.*, see Fig. 6 left, show two main features: a low-field one at the effective g-value $g_{\mathrm{eff}} = 4.3$, accompanied by a plateau extending down to the fields corresponding to $g_{\mathrm{eff}} = 9.7$, and a high-field one with $g_{\mathrm{eff}} \approx 2.0$. In early works different sharp features in the EMR spectra of glasses were assigned to distinct types of paramagnetic centres. A further progress has resulted in the concept of distribution of the spin Hamiltonian parameters caused by short-range disorder in the glass. Sharp features occur at magnetic field values stationary with respect to the parameter variations. In the case of the $^6S_{5/2}$ ions (Mn^{2+}, Fe^{3+}) the low-field features are due to ions at heavily distorted rhombic sites. The effective g-values for such ions are isotropic for the central Kramers' doublet, $g_{\mathrm{eff}} = 30/7 \approx 4.3$, and highly anisotropic for the upper and lower doublets, $g_{\mathrm{eff}_x} = \frac{6}{7} \approx 0.86$, $g_{\mathrm{eff}_y} \approx 0.61$ and $g_{\mathrm{eff}_z} \approx 9.7$ [28, 72], the latter g-value gives rise to the above-mentioned plateau. The $g_{\mathrm{eff}} = 4.3$ feature is less often reported for Mn^{2+} in glasses, a fact that is readily explained in the framework of the superposition model. Indeed, the model potential $\bar{b}_2$, determining the size of the zero-field splitting (ZFS) spin Hamiltonian parameters for given structural distortions, is much lower for Mn^{2+} in comparison with Fe^{3+} [77]. Therefore, comparable distortions result in weaker ZFS parameters for the former ion.

In sample 1 containing no Mn impurity, the $g_{\mathrm{eff}} = 4.3$ feature is due to Fe^{3+} ions. In Mn-doped samples the $g_{\mathrm{eff}} = 4.3$ feature is also due mainly to Fe^{3+}. Besides, in these samples a gradual increase in the derivative of absorption with the magnetic field is observed instead of the low-field plateau, and the slope of this increase correlates with the manganese contents showing a contribution of Mn^{2+} to this feature. The $g_{\mathrm{eff}} \approx 2.0$ feature in the Mn-doped samples is much larger than in sample 1 and shows an ill-resolved hyperfine splitting characteristic of a nuclear spin $I = \frac{5}{2}$, so, it is mainly due to Mn^{2+} ions.

The evolution of the EMR spectra with temperature has been very similar in all as-prepared samples except for sample 5 and to a lesser extent 7. The spectra intensities in Fig. 6 left have been multiplied by the absolute temperature T, so that to demonstrate the validity of the Curie law, as

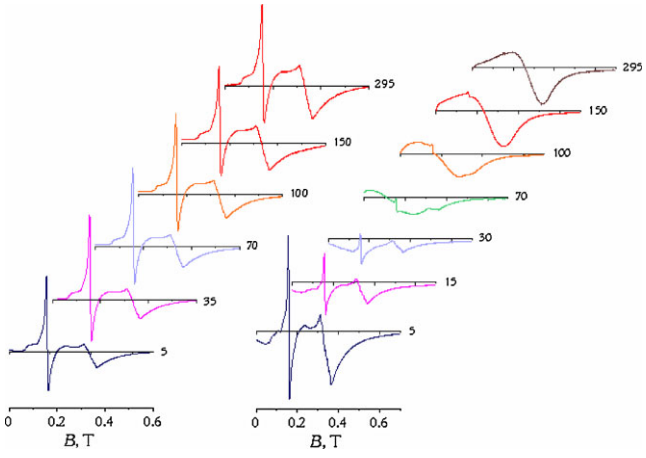

Figure 6 (online colour at: www.pss-b.com) Evolution with temperature of the EMR spectra of sample 3. The measurement temperatures (in K) are indicated alongside the curves. Left: as-prepared glass; the intensities are multiplied by absolute temperatures. Right: thermally treated glass; the intensities are plotted as measured.

expected for the EPR of diluted paramagnetic ions. The only significant change between liquid helium and room temperatures consisted in a decrease in the relative amplitude of the $g_{\mathrm{eff}} = 4.3$ feature in comparison with that of the $g_{\mathrm{eff}} \approx 2.0$ one. This can be related to a decrease in the ZFS parameters as temperature increases, as reported for a number of crystals, e.g., see Ref. [78].

We have carried out numerical simulations of the Fe^{3+} EPR spectra using a laboratory-developed *ab initio* code [15, 29]. The structural position occupied by this ion in oxide glasses has been a subject of a long-standing discussion, primarily focused on two possible coordinations, fourfold and sixfold; besides, fivefold coordination can be inferred. Figure 7 shows computer-generated spectra of Fe^{3+} assuming Gaussian random variations of interatomic distances and bond angles in the first coordination sphere of Fe^{3+} with variances 0.06 Å and 0.5°, respectively. The spectrum for the sixfold coordination clearly shows a smooth plateau in the low magnetic field range, similar to that observed in the experimental spectra. The agreement with the experiment is worse for the fivefold coordination, and in the case of the fourfold coordination a concavity occurs in this spectral range; to our knowledge, such concavity has never been observed in the EPR spectra of glasses. Besides, the experimental Fe^{3+} EPR spectra in comparison with the computer simulated ones show a marked broadening, and the hyperfine structure in the Mn^{2+} spectra is poorly resolved. This broadening infers a considerable dipole-dipole coupling of the paramagnetic ions.

Figure 8 left shows the EMR spectra at different temperatures for as-prepared sample 5. Note that in contrast to the corresponding data for sample 3 (see Fig. 6 left), those for sample 5 have *not* been corrected for the T^{-1} Curie law; therefore, the latter data show true relative

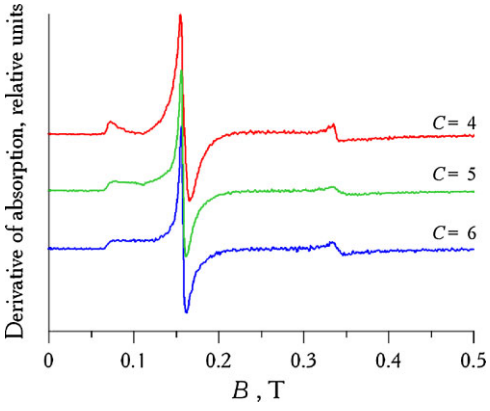

Figure 7 (online colour at: www.pss-b.com) Examples of computer-simulated EPR spectra for different coordinations of Fe^{3+}. See text for the simulation parameters.

resonance intensities at different temperatures. One can see that, unlike that of the $g_{\text{eff}} = 4.3$ feature, the overall intensity of the $g_{\text{eff}} \approx 2.0$ feature does not follow the Curie law. (We remind the reader that the thumbnail estimate of the EMR intensity is the amplitude multiplied by the square of the linewidth.) Besides, at higher temperatures the dramatic increase in intensity of the $g_{\text{eff}} \approx 2.0$ feature is accompanied by a spectacular narrowing. This clearly indicates a new type of EMR which can be identified as the SPR of magnetically ordered nanoparticles, such as previously observed for superparamagnetic nanoparticles in *thermally treated* borate glasses, *vide infra*.

In sample 7, as well, the relative intensity of the $g_{\text{eff}} \approx 2.0$ feature more rapidly increases with increasing temperature than in samples 1–4 and 6; besides, a 'two-line pattern' is developing at higher temperatures, suggesting the presence of magnetic nanoparticles (to a lesser extent than in sample 5).

The intensity of the SPR in sample 5 at higher temperatures is several orders of magnitude greater than that of the EPR of diluted ions, so, by subtracting the latter contribution from the experimental EMR spectra, the SPR contribution can be restored with sufficient accuracy. The normalized difference spectra obtained by this procedure are shown in Fig. 8 right. We have carried out computer simulations of the SPR spectra series using the previously described approach [15–17, 29]. On the basis of the results obtained using a combination of various experimental techniques, see Ref. [2], the nature of the nanoparticles was assumed as that of a non-stoichiometric manganese ferrite. A log–normal distribution of the nanoparticle sizes was used, and a spheroidal approximation was adopted for the nanoparticle shape, characterized by the respective demagnetizing factors $N_{\parallel} = \frac{1}{3} + n_{\parallel}$ and $N_{\perp} = \frac{1}{3} - \frac{1}{2}n_{\parallel}$ for particles magnetized parallel and perpendicular to the major axes.

The best-fit computer-generated spectra are shown by triangles in Fig. 8 right. Quite satisfactory fits have been obtained without taking into account the contribution of the surface anisotropy (the third term in the right-hand side of Eq. (4)). The best-fit joint distribution density of the nanoparticle sizes and demagnetizing factors $P\left(d, n_{\parallel}\right)$, shown in Fig. 9 left, has the following parameters: the most probable diameter $d_0 = 3.2$ nm, the logarithmic standard deviation of diameters $\sigma_d = 0.40$, a zero mean value of the demagnetizing factor $n_0 = 0.0$ and the corresponding distribution width $\sigma_n = 0.045$. No correlation between the size and shape distributions could be detected. From trial-and-error simulations, the accuracy of determining the distribution parameters was evaluated as being better than 10%. The marginal distribution $P_{\text{m}}(d)$, see Fig. 9 centre, is relatively broad, and the marginal distribution $P_m\left(n_{\parallel}\right)$, see Fig. 9 right, displays considerable non-sphericity of statistical nature, with no particular penchant for prolate or oblate shapes.

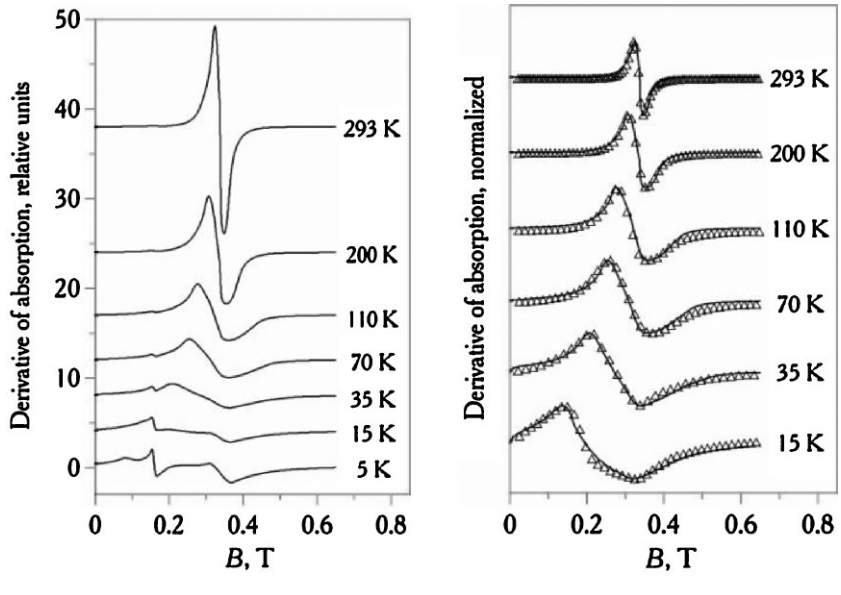

Figure 8 EMR spectra in as-prepared sample 5 at different temperatures shown alongside the curves. Left: experimental spectra. The relative intensities are plotted as measured. Right: experimental spectra after subtracting the contributions of diluted paramagnetic ions and normalization (full lines) and best-fit computer-generated spectra (triangles).

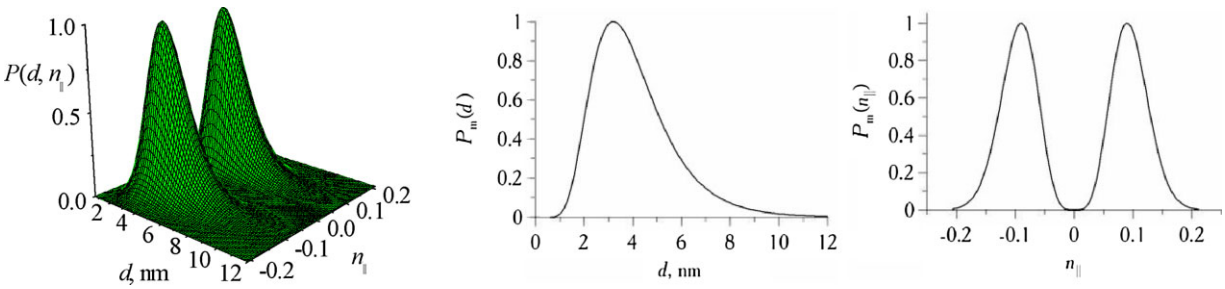

Figure 9 (online colour at: www.pss-b.com) Distribution of nanoparticle morphological parameters extracted from simulations of the SPR spectra of nanoparticles in as-prepared sample 5. Left: joint distribution density of diameters and demagnetizing factors. Centre: marginal distribution of diameters. Right: marginal distribution of demagnetizing factors. See text for the simulation parameters.

Figure 10 shows the temperature dependences of the saturation magnetization M_s and the first order magneto crystalline anisotropy K_1 extracted from the simulations. One can see that at low temperatures, M_s is close to that of the bulk manganese ferrite at 0 K, $M_s(0) = 5.6 \times 10^5$ A/m, [79]; however, it sharply decreases with the rise of temperature, suggesting a deviation from the normal Bloch law, with exponent close to 2 instead of 3/2 and the Curie temperature T_C considerably lower than in bulk manganese ferrite. Interestingly, such behaviour was predicted in the mean-field calculation of finite-size effects by Hendriksen et al. [80]. Meanwhile, in the experimental studies of the temperature dependence of M_s for manganese ferrite nanoparticles, depending on the technique of preparation and thermal treatment, two opposite tendencies have been observed, *viz*., a decrease [81, 82] and an increase [83] of T_C with a decrease in the particle size. Both tendencies have been related to finite-size effects and/or the cation redistribution between lattice sites.

The temperature dependence of K_1 is qualitatively quite similar to that reported in the literature for non-stoichiometric manganese ferrite $Mn_xFe_{3-x}O_4$ with $1.55 < x < 1.80$, see Fig. 1 in Ref. [85]. However, the absolute values of K_1 in the present study are roughly twice as large as those quoted in this work. In this context, it is worth noting that for cobalt ferrite nanoparticles the anisotropy constants are also much larger than for bulk material [86, 87].

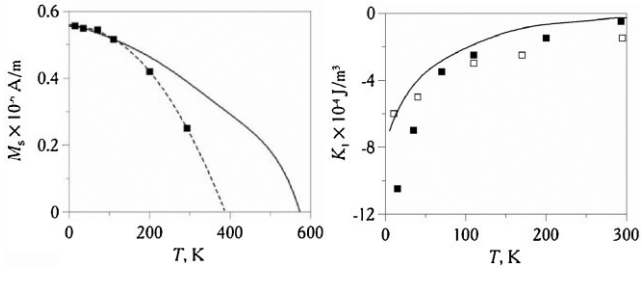

Figure 10 Temperature dependences of the magnetic parameters extracted from the computer simulations of the EMR spectra of sample 5. Left: saturation magnetization (full squares). The full curve has been calculated using the values of the saturation magnetization and the Curie temperature and Fig. 32.8 of Ref. [79]. The dashed curve is the best-fit equation $M_s = 0.56 \times 10^6 (1 - T/365.5)^{1.96}$. Right: the first-order anisotropy constant for as prepared (full squares) and heat-treated (empty squares) sample 5. The full curve has been calculated using that shown in the left graph and the K_1/M_s dependence in Fig. 1 of Ref. [84].

Thus, in the glass system studied magnetically ordered clusters occur already at the first stage of the glass preparation. In particular, magnetic nanoparticles with characteristics close to those of manganese ferrite are formed for the ratio of the Fe and Mn oxides in the charge of 3/2, as is the case for sample 5. This result is in perfect agreement with the FR data.

3.3.2 Thermally treated samples For samples 1–4 thermal treatment produces no significant change in low temperature EMR spectra; on the other hand, their room temperature spectra become very different in comparison with those of the as-prepared samples, *cf*. the spectra series for sample 3 in the left and in the right parts of Fig. 6. As temperature increases, a new large resonance line, centred at relatively low magnetic field, appears, gradually narrows and shifts to higher fields. At low temperatures this line is almost imperceptible in the EMR spectra because of its broadness, *cf*. Fig. 6 right and left. Similar but much weaker resonance is observed in thermally treated samples 1, 2 and 4.

In the series plotted in the right part of Fig. 6, the spectra intensities at different temperatures have *not* been multiplied by T, so, one can clearly see that the intensity of the new resonance does not follow the Curie law; indeed, at room temperature this intensity is several orders of magnitude greater than that of the EPR of remaining diluted ions, while the concentrations of ions contributing to these two resonances are comparable. Therefore, the new resonance can be identified as the SPR of magnetically ordered nanoparticles.

Figure 11 compares the amplitudes of the $g_{eff} = 4.3$ and $g_{eff} \approx 2.0$ features in as-prepared and thermally treated samples at liquid helium temperature (in which case there is no perceptible contribution of the EMR of nanoparticles, *cf*. Fig. 6 left and right. One can see that the reduction in the EPR intensity is more pronounced for the $g_{eff} = 4.3$ feature

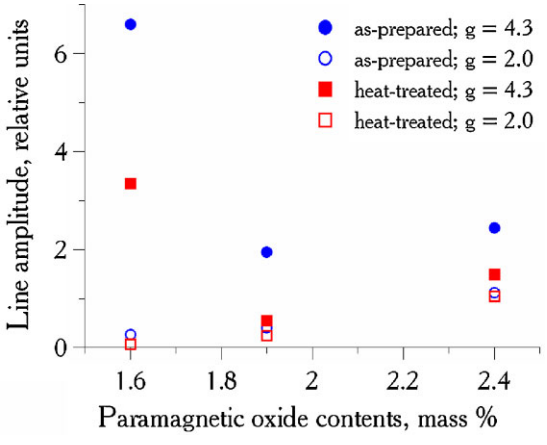

Figure 11 (online colour at: www.pss-b.com) Amplitudes of the $g = 4.3$ and $g = 2.0$ features in as-prepared and thermally treated samples.

(mainly due to Fe^{3+}) than for the $g_{eff} \approx 2.0$ one (mainly due to Mn^{2+}). This fact offers an argument in favour of magnetite as the most likely nature of the nanoparticles in thermally treated sample, as also suggested from the FR data.

We have computer simulated the SPR of nanoparticles in thermally treated sample 3 using the same formalism as before [15–17, 29]. Figure 12 shows the simulation results assuming the magnetic parameters of Fe_3O_4, $M = 480\,\mathrm{kA\,m^{-1}}$ and $K_1 = -12.8\,\mathrm{kJ\,m^{-3}}$ (cubic symmetry) [88]. The computer-generated spectrum has been obtained with the following parameters of the joint distribution density of nanoparticle sizes and demagnetizing factors: $d_0 = 3.2$ nm, $\sigma_d = 0.15$, $n_0 = 0.0$, $\sigma_n = 0.18$ and a correlation coefficient $\rho = 0.4$ between the size and shape distributions.

Figure 13 left shows the variation with temperature of the EMR spectra in sample 5 after a two-step treatment. A similar evolution is observed in thermally treated samples 8 and 9.

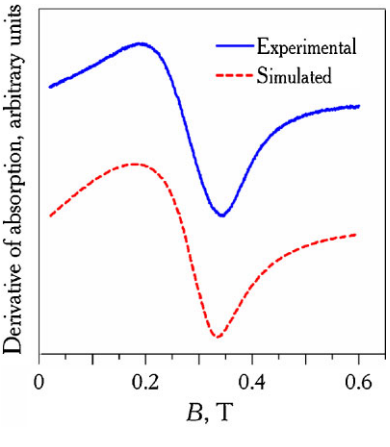

Figure 12 (online colour at: www.pss-b.com) Simulation of the difference spectrum of thermally treated sample 3 at room temperature.

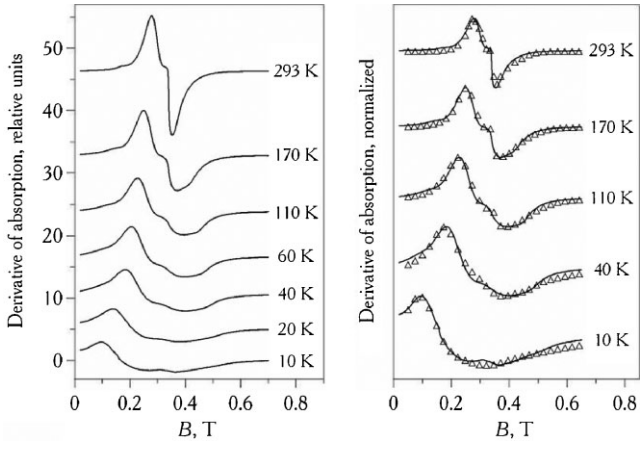

Figure 13 EMR spectra in thermally treated sample 5 at different temperatures shown alongside the curves. Left: experimental spectra. The relative intensities are plotted as measured. Right: normalized experimental spectra (full lines) and best-fit computer-generated spectra (triangles). The discrepancy between the experimental and calculated spectra at 10 K in the field range about 0.3 T is due to a superposition of the EPR of diluted Mn^{2+} ions.

Sample 5 offers a unique possibility of comparing the EMR characteristics due to the nanoparticles arising in both as-prepared and thermally treated glass. A comparison between the left parts of Figs. 8 and 13 highlights drastic changes in the temperature dependence of the spectra brought about by the thermal treatment. In the latter case, already at liquid helium temperature the broad absorption arising from magnetic nanoparticles largely predominates over the $g_{ef} = 2.0$ and $g_{ef} = 4.3$ features due to diluted Fe^{3+} and Mn^{2+} ions. The superparamagnetic nature of the EMR spectra is attested by the temperature-induced narrowing of the spread in the resonance magnetic fields; meanwhile, this narrowing is less spectacular in comparison with the as-prepared sample. Thus, a qualitative comparison between the EMR spectra in as-prepared and thermally treated sample 5 suggests larger average size and distribution of the morphological characteristics of the magnetic particles in the latter case. This distinction can be explained by the fact that in the course of thermal treatment the diluted paramagnetic ions are both joining already existing nanoparticles and forming new ones.

The above interpretation is further corroborated by computer simulations shown in Fig. 13 right. Sufficiently close fits to the experimental EMR spectra have been obtained with the saturation magnetization following the same temperature dependence as in as-prepared sample 5, see Fig. 10 left. On the other hand, the first-order magneto crystalline anisotropy K_1 in the heat-treated sample 5 in comparison with the as-prepared one shows smaller absolute values at lower temperatures and larger absolute values at higher temperatures, so that the overall temperature dependence of K_1 is weakened, see Fig. 10 right. Compared with Fig. 1 in Ref. [85], this finding suggests that the additional thermal treatment favours the formation of more

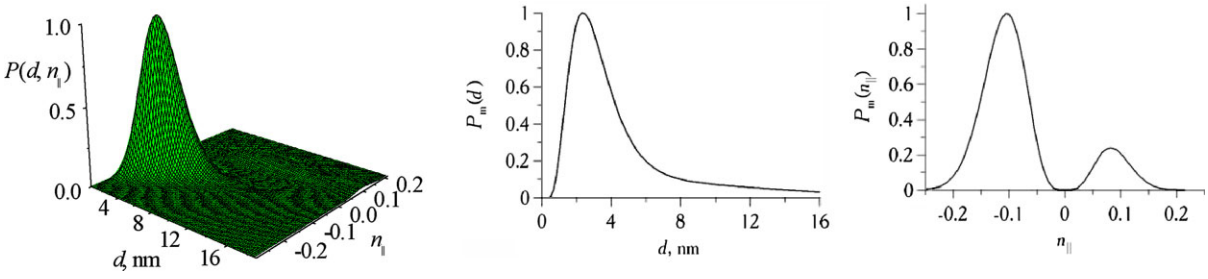

Figure 14 (online colour at: www.pss-b.com) Distribution of nanoparticle morphological parameters extracted from the simulation of the nanoparticle SPR spectrum in thermally treated sample 5. Left: joint distribution density of diameters and demagnetizing factors. Centre: marginal distribution of diameters. Right: marginal distribution of demagnetizing factors. See text for the simulation parameters.

stoichiometric $Mn_xFe_{3-x}O_4$ nanoparticles, with x values closer to 1.

In addition, in order to obtain convincing fits to the whole series of the experimental EMR spectra of thermally treated sample 5 at different temperatures, it has proven necessary to take into account a considerable contribution of the surface anisotropy, see Eq. (4). The surface anisotropy constant has been evaluated as $K_S = 2.5 \times 10^{-5}$ J/m^2 at 10 K and $K_S = 1.3 \times 10^{-5}$ J/m^2 at room temperature. Interestingly, these values are close to those found from EMR studies of maghemite nanoparticles in ferrofluids [62].

The parameters of the best-fit joint distribution density of the nanoparticle sizes and demagnetizing factors $P\left(d, n_{\|}\right)$ illustrated in Fig. 14 left, are as follows: $d_0 = 4.0$ nm, $\sigma_d = 0.55$, $n_0 = -0.04$ and $\sigma_n = 0.054$; besides, an important correlation is observed between the size and shape distributions, with the correlation coefficient $\rho = 0.6$. The marginal distribution $P_m(d)$ is significantly broadened in comparison with the as-prepared sample 5, *cf.* the central parts of Figs. 9 and 14. Still greater changes are apparent in the marginal distribution $P\left(n_{\|}\right)$, *cf.* the right parts of Figs. 9 and 14. In the heat-treated sample the latter distribution displays a marked average non-sphericity showing a certain preference for *prolate* shapes. The quoted best-fit simulation parameters have been determined with a precision of *ca.* 10%.

The large distribution of nanoparticle sizes and shapes found in thermally treated sample 5 is consistent with the transmission electron microscopy finding of a very heterogeneous particle assembly arising in this sample [2]. However, this comparison should be taken with some caution; strictly speaking, such an assembly can no more be considered as the one of non-interacting single-domain particles.

Computer simulations of the EMR spectra of other thermally treated samples are in progress, and the corresponding results will be published elsewhere.

4 Conclusion In this paper we have focused on the results obtained with two complementary experimental techniques – an 'integral' one (the Faraday rotation) and a 'local' one (the EMR). Combining these techniques yields comprehensive data on the phase state of the paramagnetic ions in the glasses. The Faraday rotation studies directly highlight exciting magneto-optical characteristics of the glasses; besides, they provide information on magnetic nature of the nanoparticles formed. On the other hand, the computer-assisted EMR studies provide insight into both the morphological and magnetic characteristics of the nanoparticles; moreover, this technique allows evaluation of the nanoparticle morphological characteristics, in particular, those of the joint distribution density of particle sizes and shapes.

The glasses described in the present work – potassium–alumina–borate glasses of molar composition $22.5K_2O$–$22.5Al_2O_3$–$55B_2O_3$ co-doped with low concentrations of Fe_2O_3 and MnO – possess the following characteristics.

(i) In as-prepared samples the majority of the paramagnetic ions are in diluted state, exhibiting FR spectra typical of weakly paramagnetic systems and characteristic EPR spectra of Mn^{2+} and Fe^{3+} ions. However, at a particular ratio of Fe and Mn oxides magnetic nanoparticles with characteristics close to those of manganese ferrite are formed already at this stage.

(ii) After thermal treatment these glasses acquire a non-linear magnetic field dependence of magnetization with hysteresis and magnetic saturation. The EMR spectra indicate the genesis and development of magnetic nanoparticles in the glass matrix.

(iii) The thermally treated glasses remain highly transparent in a part of the visible and near infrared spectral range; besides, they acquire excellent magneto-optical characteristics in the near infrared, in particular, a high absolute value of the Faraday rotation in relatively low magnetic fields. The presence of a large remnant Faraday rotation in these glasses allows keeping the light wave azimuth after switching off the magnetic field.

(iv) The EMR data show that morphology of nanoparticles formed in the glasses is characterized by the mean diameter of *ca.* 3.5–4, relatively broad size distribution of log-normal shape and considerable non-sphericity.

The extraordinary physical properties of the 'transparent magnets' – the glasses described in the present paper – in combination with their chemical stability and compatibility with glassy elements of various optical devices, suppleness and comparatively low cost of the glass technology make them good candidates for new optical and magneto-optical applications.

Acknowledgements This work is supported in part by RFBR-CNRS joint project, grant No 07-02-92174. We are grateful to E. Petrakovskaja and O. Ivanova for measuring and discussing, respectively, the EMR spectra in thermally treated samples and the FR spectral and magnetic field dependences.

References

[1] S. A. Stepanov, G. T. Petrovskii, T. V. Zarubina, E. E. Kornilova, and I. S. Edelman, Opticheskii Zh. (Russia) **70**, 46 (2003).
[2] J. Kliava, I. Edelman, O. Ivanova, R. Ivantsov, O. Bayukov, E. Petrakovskaja, V. Zaikovskiy, I. Bruckental, Y. Yeshurun, and S. Stepanov, J. Appl. Phys. **104**, 103917 (2008).
[3] J. Schinkel and G. W. Rathenau, in: Physics of Non-Crystalline Solids, Proceedings of the International Conference, edited by J. A. Prins (North-Holland Pub., Amsterdam, 1965), p. 215.
[4] E. J. Friebele, L. K. Wilson, A. W. Dozier, and D. L. Kinser, Phys. Status Solidi B **45**, 323 (1971).
[5] R. A. Verhelst, R. W. Kline, A. M. de Graat, and H. O. Hooper, Phys. Rev. B **11**, 4427 (1975).
[6] R. Muller and W. Schuppel, J. Magn. Magn. Mater. **155**, 110 (1996).
[7] A. Hoell, A. Wiedenmann, U. Lembke, and R. Kranold, Phys. B **276**, 886 (2000).
[8] Y.-K. Lee and S.-Y. Choi, J. Mater. Sci. **32**, 431 (1997).
[9] M. Hayashi, M. Susa, and K. Nagata, J. Magn. Magn. Mater. **171**, 170 (1997).
[10] N. Rezlescu and L. Rezlescu, Mater. Sci. Eng. **375–377**, 1273 (2004).
[11] D. D. Zaytsev, P. E. Kazin, A. V. Garshev, Y. D. Tret'yakov, and M. Jansen, Inorg. Mater. **40**, 881 (2004).
[12] R. Berger, J.-C. Bissey, J. Kliava, and B. Soulard, J. Magn. Magn. Mater. **167**, 1295 (1997).
[13] R. Berger, J. Kliava, J.-C. Bissey, and V. Baïetto, J. Phys.: Condens. Matter **10**, 8559 (1998).
[14] R. Berger, J. Kliava, J.-C. Bissey, and V. Baïetto, J. Appl. Phys. **87**, 7389 (2000).
[15] J. Kliava and R. Berger, Mol. Phys. Rep. **39**, 130 (2004).
[16] J. Kliava and R. Berger, Nanoparticles in oxide glasses: Magnetic resonance studies, in: Smart Materials for Ranging Systems, edited by J. Franse (Springer, 2006), p. 27–248.
[17] J. Kliava and R. Berger, J. Magn. Magn. Mater. **205**, 328 (1999).
[18] R. Berger, J.-C. Bissey, J. Kliava, H. Daubric, and C. Estournes, J. Magn. Magn. Mater. **234**, 535 (2001).
[19] V. I. Skorospelova and S. A. Stepanov, Izv. AN SSSR, ser. Neorg. Mater. **10**, 1864 (1974).
[20] S. A. Stepanov, Fizika i Khimija Stekla **2**, 228 (1976).
[21] G. N. Belozerskii, A. V. Kaljamin, E. E. Kornilova, G. T. Petrovskii, and S. A. Stepanov, Fizika i Khimija Stekla **10**, 289 (1984).
[22] G. W. Day and A. H. Rose, Proc. SPIE **985**, 138 (1988).
[23] G. E. Lano and C. Pinyan, Laser Focus World **31**, 125 (1995).
[24] F. Bentivegna, M. Nyvlt, J. Ferre, J. P. Jamet, A. Brun, S. Visnovsky, and R. Urban, J. Appl. Phys. **85**, 2270 (1999).
[25] T. W. Cease, J. G. Driggans, and S. J. Weikel, IEEE Trans. Power Delivery **6**, 1374 (1991).
[26] C. R. Kurkjian and E. A. Sigety, Phys. Chem. Glasses **9**, 73 (1968).
[27] D. W. Moon, J. M. Aitken, R. K. Mac Crone, and G. S. Cieloszyk, Phys. Chem. Glasses **16**, 91 (1975).
[28] E.-M. Yahiaoui, R. Berger, Y. Servant, J. Kliava, L. Čugunov, and A. Mednis, J. Phys.: Condens. Matter **6**, 9415 (1994).
[29] J. Kliava and R. Berger, Magnetic resonance spectroscopy of iron-doped glasses: From isolated ions to clusters and nanoparticles, in: Recent Research Development in Non-Crystalline Solids, Vol. 3 (Transworld Research Network, Kerala, 2003), ISBN 81-7895-090-1, p. 41–484.
[30] I. Ardelean, P. Pascuta, and V. Ioncu, Int. J. Mod. Phys. B **17**, 2633 (2003).
[31] J. Kliava, A. Malakhovskii, I. Edelman, A. Potseluyko, E. Petrakovskaja, S. Melnikova, T. Zarubina, G. Petrovskii, I. Bruckental, and Y. Yeshurun, Phys. Rev. B **71**, 104406 (2005).
[32] R. Berger, J. Kliava, E.-M. Yahiaoui, J.-C. Bissey, P. K. Zinsou, and P. Béziade, J. Non-Cryst. Solids **180**, 151 (1995).
[33] T. Komatsu and N. Soga, J. Chem. Phys. **72**, 1781 (1980).
[34] R. R. Show and J. H. Heasley, J. Am. Ceram. Soc. **50**, 297 (1967).
[35] L. K. Wilson, E. J. Frieble, and D. L. Kineer, in: Amorphous Magnetism, edited by H. O., Hooper and M. de Graaf (Plenum Press, New York, London, 1973), p. 65.
[36] K. Mandal, S. Chakraverty, S. Pan Mandal, P. Agudo, M. Pal, and D. Chakravorty, J. Appl. Phys. **92**, 501 (2002).
[37] N. Rajic, M. Ceh, R. Gabrovsek, and V. Kaucic, J. Am. Ceram. Soc. **85**, 1719 (2002).
[38] R. J. Landry, J. T. Fournier, and C. G. Young, J. Chem. Phys. **46**, 1285 (1967).
[39] T. Egami, O. A. Sacli, A. W. Simpson, and A. L. Terry, Amorphous Antiferromagnetism in Some Transition Element-Phosphorus Pentoxide Glasses, in: Amorphous Magnetism, edited by H. O. Hooper and M. de Graaf (Plenum Press, New York, London, 1973), p. 27–45.
[40] R. C. Mac Crone, Magnetic Inhomogeneities in $BaO–B_2O_3–Fe_2O_3$ oxide Glasses, in: Amorphous Magnetism, edited by H. O. Hooper and M. de Graaf (Plenum Press, New York, London, 1973), p. 77–84.
[41] R. de Bufala, Bull. Soc. Esp. Ceram. **10**, 247 (1971).
[42] E. A. Gravchikova, D. D. Zaitsev, P. E. Kazin, M. V. Popov, Y. D. Tretyakov, and M. Jansen, Inorg. Mater. **42**, 914 (2006).
[43] D. D. Zaitsev, E. A. Gravchikova, P. E. Kazin, A. V. Garshev, Y. D. Tret'yakov, and M. Jansen, Inorg. Mater. **42**, 326 (2006).
[44] K. Watanabe and K. Hoshi, Phys. Chem. Glasses **40**, 75 (1999).
[45] M. Mirkazemi, V. K. Marghussian, and A. Beitollahi, Ceram. Int. **32**, 43 (2006).
[46] M. Mirkazemi, V. K. Marghussian, A. Beitollahi, S. X. Dou, D. Wexler, and K. Konstantinov, Ceram. Int. **33**, 463 (2007).
[47] H. Akamatsu, K. Tanaka, K. Fujita, and S. Murai, J. Phys.: Condens. Matter **20**, 235216 (2008).
[48] H. Akamatsu, K. Tanaka, K. Fujita, and S. Murai, J. Magn. Magn. Mater. **310**, 1506 (2007).
[49] R. Serber, Phys. Rev. **41**, 489 (1932).
[50] P. J. Stephens, J. Chem. Phys. **52**, 3489 (1970).
[51] N. F. Borrelli, J. Chem. Phys. **41**, 3289 (1964).

[52] G. T. Petrovskii, T. V. Zarubina, A. V. Malakhoskii, V. N. Zabluda, and M. Yu. Ivanov, J. Non-Cryst. Solids **130**, 35 (1991).
[53] K. Tanaka, K. Fujita, N. Soga, J. Qiu, and K. Hirao, J. Appl. Phys. **83**, 840 (1997).
[54] T. Hayakawa, M. Nogami, N. Nishi, and N. Sawanobori, Chem. Mater. **14**, 3223 (2002).
[55] A. Potseluyko, I. Edelman, A. Malakhovskii, Y. Yeshurun, T. Zarubina, A. Zamkov, and A. Zaitsev, Microelectron. Eng. **69**, 216 (2003).
[56] H. Akamatsu, K. Fujita, S. Murai, and K. Tanaka, Appl. Phys. Lett. **92**, 251908 (2008).
[57] J. H. Van Vleck, and M. H. Hebb, Phys. Rev. **46**, 17 (1934).
[58] I. S. Edelman, O. S. Ivanova, K. P. Polyakova, V. V. Polyakov, and O. A. Bayukov, Phys. Solid State **50**, 1 (2008).
[59] I. S. Edelman and A. V. Malakhovskii, Optika i Spektroskopija **35**, 959 (1973).
[60] Z. Šimša, P. Tailhades, L. Presmanes, and C. Bonningue, J. Magn. Magn. Mater. **242–245**, 381 (2001).
[61] G. V. Skrotskii and L. V. Kurbatov, in: Ferromagnetic Resonance, edited by V. Vonsovskii (Pergamon Press, Oxford, 1966).
[62] F. Gazeau, J. C. Bacri, F. Gendron, R. Perzynski, Yu, L. Raikher, V. I. Stepanov, and E. Dubois, J. Magn. Magn. Mater. **186**, 175 (1998).
[63] R. H. Kodama and A. E. Berkowitz, Phys. Rev. **59**, 6321 (1999).
[64] L. Baselgia, M. Warden, F. Waldern, S. L. Hutton, J. E. Drumheller, Y. Q. He, P. E. Wigen, and M. Marysko, Phys. Rev. B **38**, 2237 (1988).
[65] N. Noginova, F. Chen, T. Weaver, E. P. Giannelis, A. B. Bourlinos, and V. A. Atsarkin, J. Phys.: Condens. Matter **19**, 246208 (2007).
[66] V. K. Sharma and F. Waldner, J. Appl. Phys. **48**, 4298 (1977).
[67] R. S. de Biasi, and T. C. Devezas, J. Appl. Phys. **49**, 2466 (1978).
[68] L. Yu, V. Raikher, and I. Stepanov, Sov. Phys. JETP **75**, 764 (1992).
[69] Yu. L. Raikher, and V. I. Stepanov, Phys. Rev. B **50**, 6250 (1994).
[70] W. F. Brown, Jr., IEEE Trans. Magn. **Mag-15**, 1196 (1979).
[71] E. Rezlescu, N. Rezlescu, and M. L. Craus, J. Phys. **IV–7**, 553 (1997).
[72] J. Kliava, Phys. Status Solidi B **134**, 411 (1986).
[73] M. G. Mortuza, R. Dupree, and D. Holland, J. Mater. Sci. **35**, 2829 (2000).
[74] N. K. Mohan, M. R. Reddy, M. Rami, C. K. Jayasankar, and N. Veeraiah, J. Alloys Compd. **458**, 66 (2008).
[75] C. Horea, M. Toderas, and I. Ardelean, J. Optoelectron. Adv. Mater. **9**, 708 (2007).
[76] P. V. Reddy, C. L. Kanth, V. P. Kumar, N. Veeraiah, and P. Kistaiah, J. Non-Cryst. Solids **351**, 3752 (2005).
[77] D. J. Newman and E. Siegel, J. Phys. C, Solid State Phys. **9**, 4285 (1976).
[78] W.-C. Zheng and S.-Y. Wu, J. Phys.: Condens. Matter **9**, 5081 (1997).
[79] J. Smit and H. P. J. Wijn, Ferrites, edited by N. V. Philips (Philips Technical Library, Eindhoven, The Netherlands, 1959).
[80] P. V. Hendriksen, S. Linderoth, and P.-A. Lindgård, J. Magn. Magn. Mater. **104–107**, 1577 (1992).
[81] J. P. Chen, C. M. Sorensen, K. I. Klabunde, G. C. Hadjipannayis, E. Devlin, and A. Kostikas, Phys. Rev. B **54**, 9288 (1996).
[82] C. Tsang, H. D. Gafney, D. Sunil, M. Rafailovich, J. Sokolov, and R. J. Gambino, J. Appl. Phys. **79**, 6025 (1996).
[83] M. Zheng, X. C. Wu, B. S. Zou, and Y. J. Wang, J. Magn. Magn. Mater. **183**, 152 (1998).
[84] J. F. Dillon Jr. and H. E. Earl, J. Appl. Phys. **30**, 202 (1959).
[85] W. Palmer, J. Appl. Phys. **33** (suppl), 1201 (1962).
[86] L. D. Tung, V. Kolesnichenko, D. Caruntu, N. H. Chou, C. J. O'Connor, and L. Spinu, J. Appl. Phys. **93**, 7486 (2003).
[87] A. Virden, S. Wells, and K. O'Grady, J. Magn. Magn. Mater. **316**, 768 (2007).
[88] Z. Kąkol and J. M. Honig, Phys. Rev. B **40**, 9090 (1989).